Lithuanian Journal of Physics, Vol. **62**, No. 4, pp. 243–253 (2022)

SOLID-STATE NMR STUDY OF SPIN DYNAMICS AND LOCAL DISORDER IN SMART POLYMERS: PDMAEMA

V. Klimavičius [a], V. Klimkevičius [b], L. Dagys [c], K. Aidas [a],

R. Makuška [b], and V. Balevičius [a]

[a] *Institute of Chemical Physics, Vilnius University, Saulėtekio 9, 10222 Vilnius, Lithuania*
[b] *Institute of Chemistry, Vilnius University, Naugarduko 24, 03225 Vilnius, Lithuania*
[c] *NVision Imaging Technologies GmbH, D-89081 Ulm, Germany*
Email: vytautas.balevicius@ff.vu.lt

Received 28 September 2022; accepted 3 October 2022

The solid-state ^{1}H and ^{13}C NMR spectra as well as the ^{1}H–^{13}C cross-polarization upon magic angle spinning (CP MAS) kinetics were studied for poly[2-(dimethylamino)ethyl methacrylate] (PDMAEMA), i.e. a smart pH- and thermo-responsive polymer. The stereochemical content of PDMAEMA was determined from the complex shaped ^{13}C MAS signal of CH_3 group. The kinetic data were processed using the Hirschinger and Raya spin dynamics model that includes the complete scheme of rotating frame spin-lattice relaxation pathways. The general solution was adapted for the spin cluster treatment. The earlier studied experimental CP MAS kinetics data of poly [2-(methacryloyloxy)ethyl trimethylammonium chloride] (PMETAC), i.e. one of its quaternized form, were revisited and newly processed applying this model. The spin-lattice relaxation of protons in the rotating frame in PDMAEMA and PMETAC occurs in the same scale from one to tens of milliseconds. Very high anisotropy of spin-diffusion was found for both polymers. However, the local disorder of various spin sites in PDMAEMA is significantly higher than in PMETAC. It is characterized by the order parameters 0.71–0.77 and 0.87–0.91, respectively. The main chain in PDMAEMA is also more disordered and more flexible than in PMETAC.

Keywords: solid-state NMR, cross-polarization, smart polymers, poly[2-(dimethylamino)ethyl methacrylate]

1. Introduction

Cross-polarization (CP), combined with magic-angle spinning (MAS), is one of the most widely used techniques in solid-state NMR spectroscopy [1–3]. The processing of CP kinetic data, i.e. the consideration of the time evolution (contact time) of communication between spins, provides the rates of spin-diffusion and spin-lattice relaxation, the profiles of distribution of dipolar coupling and some other parameters accounting for the effective sizes of spin clusters [4–6]. Hence, it is a powerful method studying fine structural details and dynamics in advanced complex materials and polymers among those [7–10].

In the present work, the CP MAS kinetics was applied studying a representative of a very important class of materials – smart polymers. Poly[(dimethylamino)ethyl methacrylate] (PDMAEMA) was chosen for this study for several reasons. It has a tertiary amine structure as a pendant group, which in an acidic medium or in the form of quaternary ammonium salt acquires a cationic character. PDMAEMA is known as a smart pH- and thermoresponsive polymer [11–13]. The physical properties of such polymers, like chain conformation and solubility, can be tailored by manipulating the pH, ionic strength or temperature. pH-sensitive polymers combined with nanoparticles are intended to be used in chemotherapy to overcome major problems related to tumor heterogeneity, non-specific distribution of the drugs in tissues and multidrug resistance against anticancer drugs [12, 13]. In combination with a suitable hydrophobic block,

PDMAEMA enables formation of micelles [14]. Micelles have gained significant attention since they can be used to encapsulate and subsequently release compounds, which is very important in drug delivery. However, PDMAEMA is susceptible to hydrolysis, therefore its quaternized form, containing a permanent charge, is preferred in water-based applications [14]. Interactions between water molecules and PDMAEMA are more complex than those occurring in the most nonionic thermoresponsive polymers [11]. Water solubility of atactic PDMAEMA is strongly pH-dependent. Quaternized PDMAEMA is a versatile polymer that can be applied in antimicrobial systems, such as films with porous surfaces of narrow size, cationic coatings for silica nanoparticles, recognition elements against bacteria, tandem systems with fungicide properties, and as a material for antibacterial fibres or nanocrystals [15]. PDMAEMA-based advanced materials with well-defined compositions, architectures and functionalities are promising for gene transfection [16].

The purpose of the present work was to study ^{1}H–^{13}C CP MAS kinetics in PDMAEMA determining the rates of spin-diffusion processes and spin-lattice relaxation in the rotating frame, and also the dipole–dipole coupling constants and the local dynamic order parameters for various molecular segments. An especial interest was to compare the solid-state NMR data for PDMAEMA and its quaternized derivative PMETAC evaluating the local disorder and chain flexibility in both polymers.

2. Experiment

Poly[2-(dimethylamino)ethyl methacrylate] (PDMAEMA) was synthesized via radical addition-fragmentation chain transfer (RAFT) polymerization according to previously published data with minor adjustments [17, 18]. Polymerization of DMAEMA was carried out in 1,4-dioxane (DO) in the presence of 4,4-azobis(4-cyanovaleric acid) (ACVA, 98%, *Fluka*) as an initiator and 4-(((butylthio)carbonothioyl)thio)-4-cyanopentanoic acid as a highly efficient RAFT chain transfer agent (CTA) [19]. Shortly, DMAEMA (1.57 g, 10 mmol), RAFT CTA (0.014 g, 0.05 mmol) and ACVA (0.0046 g, 0.016 mmol) were placed into a round-bottomed 25 mL flask equipped with a magnetic stirrer and dissolved in 15.4 mL of DO. The stirred solution was bubbled for 30 min under argon gas, sealed and heated at 70°C. The copolymerization reaction was carried out for 24 h and then quenched by cooling the flask down to –80°C and opening to the air. The copolymers were separated and purified by precipitation into cold diethyl ether. The reaction products are yellowish to white powder, yield 89%. The chemical structure of PDMAEMA is shown in Fig. 1.

The solid-state NMR experiments were carried out on a *Bruker* AVANCE III HD spectrometer using a 4 mm double resonance CP MAS probe. The experiments were performed at 298 K in 9.4 T magnetic field using an Ascend wide bore superconducting magnet. The resonance frequencies of the ^{1}H and ^{13}C nuclei are 400.2 and 100.6 MHz, respectively. The samples were spun at magic-angle at the rate of 10 kHz using a 4 mm zirconia rotor. To fulfill one of the Hartmann–Hahn matching conditions in CP MAS experiments, rectangular (63 kHz RF field for ^{13}C) variable contact time pulses were used. In the present work, all experiments were adjusted to fulfill the $n = +1$ condition. The experimental and computed ^{13}C CP MAS spectra of PDMAEMA are shown in Fig.1. The CP MAS kinetics were recorded by varying the contact times from 50 μs to 10 ms in increments of 25 μs. The ^{1}H–^{13}C CP MAS FSLG HETCOR spectra (Fig. 2) were measured using 128 scans per 128 increments using a short (70–100 μs) ramped (50–100%) CP contact. All spectra were referenced to TMS using adamantane as an external reference ($\delta(^{1}\mathrm{H}) = 1.85$ ppm, $\delta(^{13}\mathrm{C}) = 38.52; 29.47$ ppm). NMR spectra were processed using the Topspin 3.2 software. Some additional processing was carried out using the Microcal Origin and MathCad packages.

3. DFT calculations

Calculations of NMR isotropic magnetic shielding constants for ^{1}H and ^{13}C nuclei in PDMAEMA have been performed using the density functional theory (DFT). The B3LYP exchange-correlation functional in combination with the 6-311G** basis set was used for geometry optimization of isolated fragments of PDMAEMA. The magnetic shielding tensors have been calculated *in vacuo* by using the modified hybrid functional of Perdew, Burke and Ernzerhof (PBE0) along with the 6-311++G(2d,2p) basis set. The gauge-including atomic orbital (GIAO)

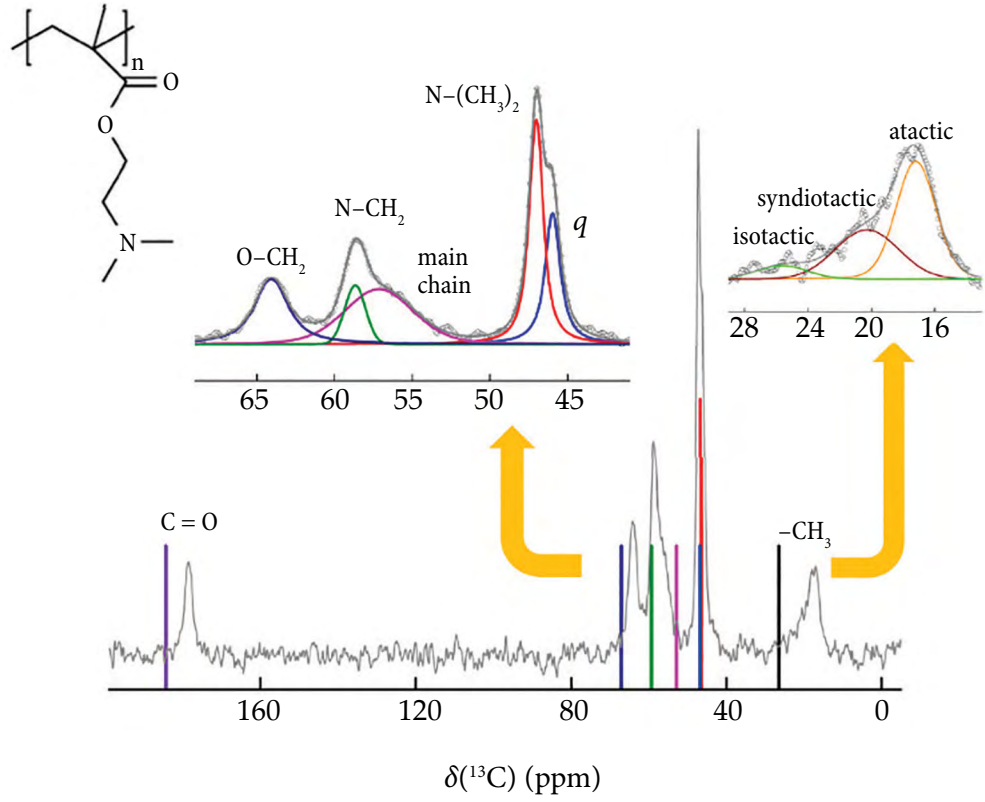

Fig. 1. The experimental and computed (vertical bars) ^{13}C CP MAS spectra of neat PDMAEMA. Note the strong overlaps of the CH_2 main chain signal with that of N-CH_2 and the quaternary carbon (q) with N-$(CH_3)_2$, respectively. The overlapped experimental contours were separated using Voigt functions. More comments in the text.

approach [20] was used to ensure the gauge invariance of the results. Gaussian 16 program [21] was used for all our calculations. The ^{1}H and ^{13}C chemical shifts were obtained by subtracting the computed isotropic shielding constants from the corresponding shielding constants of TMS taken from [22]. We have analyzed the isolated fragments of PDMAEMA composed of 2 monomers in order to support the assignment of experimentally observed signals. As seen in Figs. 1and 2, the computational results well agree with the experimental ^{1}H and ^{13}C NMR spectra.

4. Theoretical model of CP kinetics

The most widely used kinetic models that exhibit the coherent oscillatory behaviour of CP intensity originate from the pioneer work of Müller et al. [23]. The spin system is treated as a strongly coupled I*–S spin pair immersed in a spin-bath consisting of the remaining I spins (I = ^{1}H and S = ^{13}C in the present work). There it is assumed that only one spin I* interacts with the I-spin bath (or infinite energy reservoir of I spins), which is described in a phenomenological way. It was called as the I–I*–S model. Later the model was developed by Naito and McDowell [24] revealing the anisotropy of spin-diffusion processes and adding the spin-lattice relaxation of I and S spins in the rotating frame ($T^{\mathrm{I}}_{1\rho}$ and $T^{\mathrm{S}}_{1\rho}$). The topic of CP kinetics, i. e. the dependence of CP signal intensity $I(t)$ on the contact time (t), was reviewed and discussed in Refs. [1, 6, 25]. However, as it was noted in Ref. [6], the kinetic equation originally derived by Naito and McDowell [24] is *incorrect* in the presence of $T_{1\rho}$ relaxation. In the present work, the correct solution derived by Hirschinger and Raya [26] was used. In its general form this solution contains a complete scheme of the spin-lattice relaxation in the rotating frame with the rates $R^{\mathrm{I}}_{1\rho} = 1/T^{\mathrm{I}}_{1\rho}$, $R^{\mathrm{I}^*}_{1\rho} = 1/T^{\mathrm{I}^*}_{1\rho}$ and $R^{\mathrm{S}}_{1\rho} = 1/T^{\mathrm{S}}_{1\rho}$ for the spins I, I* and S, respectively, and is rather cumbersome to apply. However, it can be simplified under certain dynamic constrains. For instance, if the relaxation rates of the remote and strongly coupled protons are almost equal, i.e. $R^{\mathrm{I}}_{1\rho} \approx R^{\mathrm{I}^*}_{1\rho}$, the kinetic equation is written as

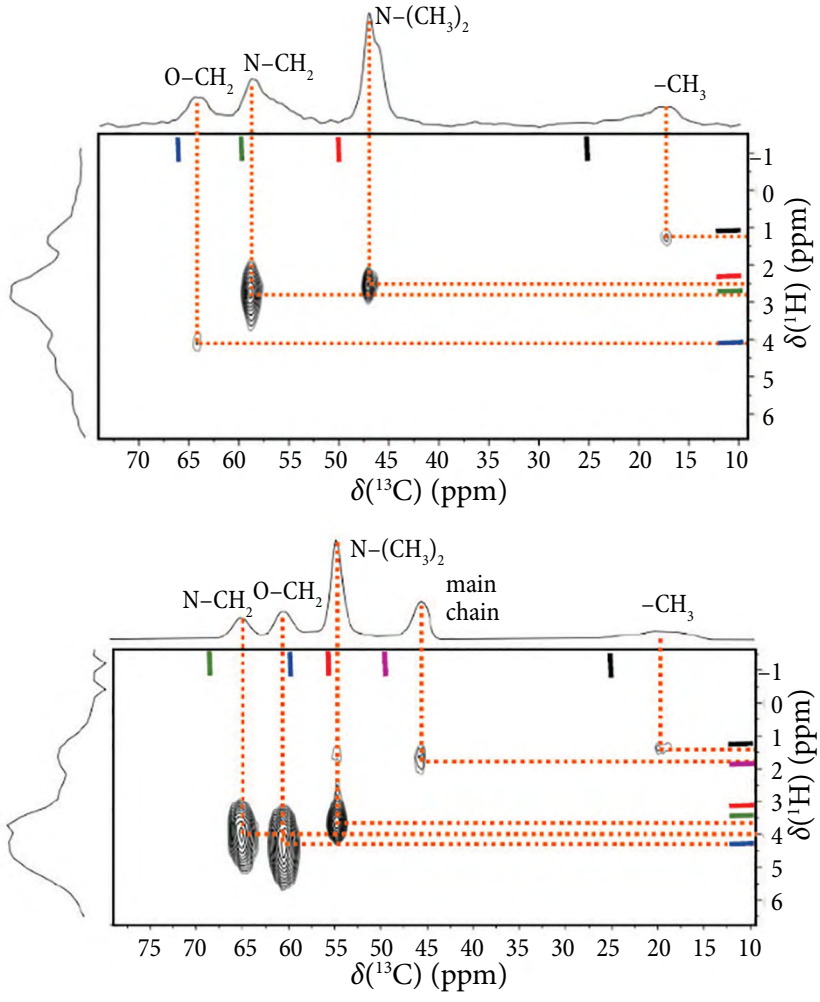

Fig. 2. Comparison of ^{1}H–^{13}C CP MAS frequency switched Lee–Goldberg (FSLG)-heteronuclear correlation (HETCOR) spectra of PDMAEMA (upper panel) and PMETAC (lower panel). The DFT calculated ^{1}H and ^{13}C chemical shifts are shown by the horizontal and vertical bars, respectively. The experimental and calculated carbonyl signals are out of the present scale and not shown. More comments in the text.

$$I(t) = I_0 \left\{ \left[\frac{1}{2} - \frac{R^{\Sigma}_{\mathrm{df}}}{R^{\Sigma}_{\mathrm{df}} + R^{\mathrm{S}}_{1\rho}/2 - R^{\mathrm{I}}_{1\rho}/2} \right] \mathrm{e}^{-\left(R^{\Sigma}_{\mathrm{df}} + R^{\Sigma}_{1\rho}/2\right)t} + \left(\frac{R^{\Sigma}_{\mathrm{df}}}{R^{\Sigma}_{\mathrm{df}} + R^{\mathrm{S}}_{1\rho}/2 - R^{\mathrm{I}}_{1\rho}/2} \right) \mathrm{e}^{-R^{\mathrm{I}}_{1\rho} t} - \frac{1}{2} \mathrm{e}^{-\left(R^{\Sigma}_{\mathrm{df}} + R^{\mathrm{I}}_{\mathrm{dp}}/2 + R^{\Sigma}_{1\rho}/4\right)t} \left\langle \cos(b\,t) \right\rangle_{\mathrm{AA}} \right\}, \tag{1}$$

where $R^{\mathrm{I}}_{\mathrm{dp}}$ and $R^{\mathrm{I}}_{\mathrm{df}}$ are the (homonuclear) spin-diffusion rate constants of the I* spin, $R^{\mathrm{S}}_{\mathrm{df}}$ is that of the S spin (heteronuclear), $R^{\Sigma}_{\mathrm{df}} = R^{\mathrm{I}}_{\mathrm{df}} + R^{\mathrm{S}}_{\mathrm{df}}$ (the physical meaning of the rate constants $R^{\mathrm{I}}_{\mathrm{dp}}$, $R^{\mathrm{I}}_{\mathrm{df}}$ and $R^{\mathrm{S}}_{\mathrm{df}}$ was thoroughly discussed in [1, 27, 28]), $R^{\Sigma}_{1\rho} = R^{\mathrm{I}}_{1\rho} + R^{\mathrm{S}}_{1\rho}$, and the brackets $\langle \ldots \rangle_{\mathrm{AA}}$ mean the angular averaging [6, 29]. The cosine-oscillation frequency b (Eq. (1)) depends on the gyromagnetic ratios (γ_{I}, γ_{S}) of the two interacting nuclei (I and S), the distance r between them and the angle θ between the $\boldsymbol{r}$ vector and the magnetic field

$$b = \frac{\mu_0}{4\pi} \frac{\gamma_{\mathrm{I}} \gamma_{\mathrm{S}} h}{r^3} \frac{(3\cos^2\theta - 1)}{2} = D_{\mathrm{IS}} P_2(\cos\theta), \tag{2}$$

where D_{IS} is the heteronuclear I–S dipolar coupling constant $D_{\mathrm{IS}} = (1/2\pi)\,(\mu_0/4\pi)\,\gamma_{\mathrm{I}}\gamma_{\mathrm{S}}\,(h/2\pi)/r^3$ (in Hz).

As the dipolar splitting b is an 'angular' function, the proper angular averaging has to be performed in order to adapt this equation to powder samples [5, 29]. The angular averaging (AA) for CP experiments applying MAS is carried out as

$$\langle \cos(b_n t)\rangle_{\mathrm{AA}} = \frac{1}{2}\int_0^{\pi} \cos(b_n(\beta)t)\sin(\beta)\mathrm{d}\beta, \qquad (3)$$

where β is the polar angle between the $\boldsymbol{r}$ vector and the MAS rotor axis [29]. Depending on the HH matching condition $\omega_{1\mathrm{I}} - \omega_{1\mathrm{S}} = n\omega_{\mathrm{MAS}}$ is fulfilled ($n = \pm 1$, the present work), the AA procedure has to be carried out on the $\cos(b_n t)$ oscillation that contains the spherical components of the b-tensor

$$b_{\pm 1} = \frac{D_{\mathrm{IS}}}{2\sqrt{2}}\sin(2\beta). \qquad (4)$$

In the present work, the angular averaging (Eq. (3)) was carried out analytically using the series of Bessel J_n functions [29, 30].

Equation (1) was successfully applied for ^{1}H–^{31}P CP MAS build-up curves in amorphous phosphates [6]. However, the I–I*–S model considers an I*–S pair. It is known that the relative amplitudes of the coherent and incoherent stages of the polarization transfer are strongly dependent on the considered spin subsystem or cluster. Therefore, in order to handle CH_2 and CH_3 groups in PDMAEMA, the treatment should be modified.

The Naito and McDowell analytical solution [24] was modified for the I$^{*}_n$–S spin clusters introducing the additional parameter λ that is related to the cluster size n [25]. If the I*–S coupling constant is much larger than the spin diffusion rate constants ($|b| \gg$) $R^{\mathrm{I}}_{\mathrm{df}}$, $R^{\mathrm{I}}_{\mathrm{dp}}$) and $R^{\Sigma}_{\mathrm{df}} \gg \mathrm{R}^{\mathrm{I}}_{1\rho}$ is valid, the modified solution is written as

$$I(t) = I_0 \mathrm{e}^{-R^{\mathrm{I}}_{1\rho}t} \left\{ 1 - \lambda \mathrm{e}^{-R^{\Sigma}_{\mathrm{df}}t} - (1-\lambda)\mathrm{e}^{-\left(\frac{1}{2}R^{\mathrm{I}}_{\mathrm{dp}} + R^{\Sigma}_{\mathrm{df}}\right)t} \langle \cos(b\,t)\rangle_{\mathrm{AA}} \right\}. \qquad (5)$$

However, as the starting equation that was used deriving Eq. (5) appeared to be incorrect, the analogue of Eq. (5) has to be derived from the corrected one (Eq. (1), or for the general formula see [26]). The mathematical recast, seeking that the final expression would be similar to the above formula, leads to

$$I(t) = I_0 \mathrm{e}^{-\mathrm{R}^{\mathrm{I}}_{1\rho}t} \{1 - \lambda \mathrm{e}^{-At} - (1-\lambda)\mathrm{e}^{-(A+B)t} \langle \cos(bt)\rangle_{\mathrm{AA}}\}, \qquad (6)$$

where the kinetic parameters A and B depend on the relaxation regime (Table 1). The 'size' parameter λ was introduced in the same manner as in Ref. [25], i.e. by replacing the relative magnitudes of the exponents of incoherent and coherent CP stages by λ and $1 - \lambda$, respectively. As λ depends on the cluster size and group mobility, it must be adjusted for each kinetics by the fitting of experimental and calculated CP build-up curves.

In the present work, the nonlinear curve fitting to experimental data was carried out using Eq. (6) and applying the Levenberg–Marquardt algorithm implemented in the Microcal Origin and MathCad packages.

5. Results and discussion

It is known that PDMAEMA can exist in three steric configurations – isotactic, atactic and syndiotactic [11]. These stereochemically different forms can be distinguished in the high resolution ^{1}H and ^{13}C NMR spectra of PDMAEMA in DMSO and $CDCl_3$ solutions [11, 14]. Unfortunately, these configurations cannot be well resolved by the solid-state NMR because of motional slow-down and the line broadening. However, the decomposition of the CH_3 signal was successful in the ^{13}C MAS spectrum into three components (Fig. 1). According to the assignment given in [11], these three peaks correspond to isotactic (25.7 ppm), syndiotactic (20.3 ppm) and atactic (17.2 ppm) conformers, respectively. The relative intensities of the peaks allow one to state that

Table 1. The kinetic parameters A and B (Eq. (6)) at various regimes of spin-lattice relaxation in the rotating frame.

Regime	A	B	Comment
$R^{\mathrm{I}^{*}}_{1\rho} = R^{\mathrm{I}}_{1\rho}$, $R^{\mathrm{S}}_{1\rho} \to 0$	$R^{\Sigma}_{\mathrm{df}} - R^{\mathrm{I}}_{1\rho}/2$	$R^{\mathrm{I}}_{\mathrm{dp}}/2 - R^{\mathrm{I}}_{1\rho}/4$	For diluted spins S and single I-bath; it is often set for ^{13}C–^{1}H pairs [25].
$R^{\mathrm{I}^{*}}_{1\rho} = R^{\mathrm{I}}_{1\rho} = R^{\mathrm{S}}_{1\rho}$	R^{Σ}_{df}	$R^{\mathrm{I}}_{\mathrm{dp}}/2 - R^{\mathrm{I}}_{1\rho}/2$	The case of the global 'isotropic' rotating frame relaxation.
$R^{\mathrm{I}^{*}}_{1\rho} \approx R^{\mathrm{S}}_{1\rho} \neq R^{\mathrm{I}}_{1\rho}$	R^{Σ}_{df}	$R^{\mathrm{I}}_{\mathrm{dp}}/2 + R^{\mathrm{I}^{*}}_{1\rho}/2 - R^{\mathrm{I}}_{1\rho}$	In the case of very strong I*–S coupling both spins relax with the near rates.

the PDMAEMA synthesized via RAFT polymerization is predominantly atactic (56%) with a comparable amount of the syndiotactic form (36%). The isotactic form is present in a much lower concentration (ca 8%).

Because of the line broadening and strong overlap (Fig. 1) the $^{1}H–^{13}C$ CP MAS kinetics in PDMAEMA were studied only for three different spin sites, viz. O-CH_2 (64 ppm), N-CH_2 (59 ppm) and N-$(CH_3)_2$ (47 ppm). The build-up kinetic curves for them are presented in Fig. 3. The high-density experimental data set allows one to reduce the excessive freedom in the non-linear curve fitting that increases the stability of the flow towards the 'true' minimum on the multi-parameter surface χ^2, i.e. to the minimal sum of weighted squares of deviations of the chosen theoretical model curve from the experimental one.

The nonlinear curve fitting was carried out using Eq. (6) on the six parameters surface $\chi^2(A, B, b, R^I_{1\rho}, \lambda, I_0) \rightarrow minimum$. The fitted parameters are presented in Table 2.

$B \gg A$ was found for all studied spin sites (Table 2). This means that $R^I_{dp} \gg R^{\Sigma}_{df}$ at any relaxation regime (Table 1) and the spin diffusion in PDMAEMA is highly anisotropic. It looks that the Ising-type interaction ($R^I_{df} = R^S_{df} = 0$) should be dominant. An exceptional situation may arise in the case of a very fast relaxation of I^* spins, i.e. $R^{I^*}_{1\rho} \gg R^I_{1\rho}$. Unfortunately, the precision of the separate determination of $R^{I^*}_{1\rho}$ and $R^S_{1\rho}$ is rather low as the sum of R^{Σ}_{df}, $R^{I^*}_{1\rho}$ and $R^S_{1\rho}$ appears in the general kinetic equation [26]. This is not the case for the relaxation rate of I-protons $R^I_{1\rho}$, because it solely drives the exponential decay of the magnetization through the second term (Eq. (1)).

For polycrystalline as well as for powder materials, the destructive interference of the orientation-dependent coherences significantly contributes to the decay of transient oscillations. Thus, the calculations implementing the angular averaging (Eq. (6)) should provide a more accurate evaluation of the spin-diffusion rates and the dipole–dipole coupling constants. Analysis of the dipole–dipole coupling strength allows the identification of dynamic disordering in the sample [31]. The local dynamic order parameter S is defined as the ratio of the experimental dipolar coupling constant and the calculated static dipolar coupling constant [32–35]

$$S = \frac{D_{CH}}{D_{stat}} = \langle P_2(\cos\alpha)\rangle, \qquad (7)$$

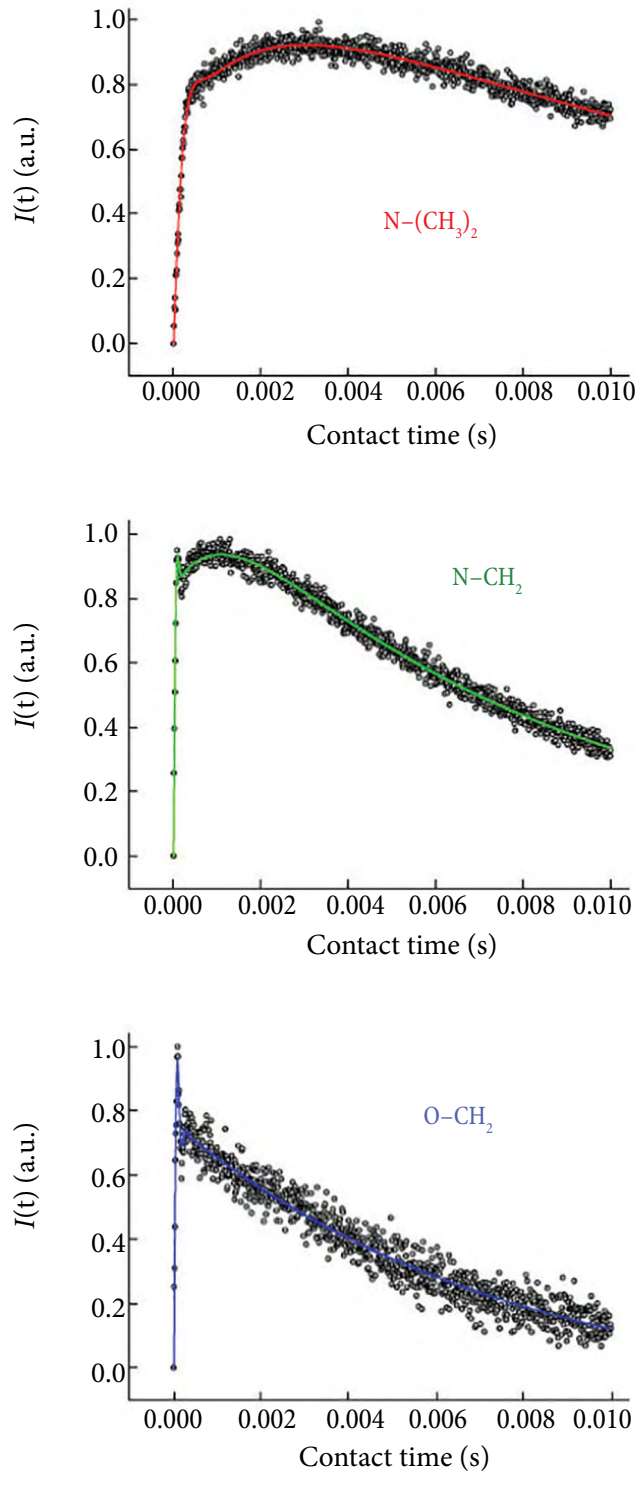

Fig. 3. The experimental $^{1}H–^{13}C$ CP MAS kinetics (circles) for various spin sites in PDMAEMA at 10 kHz MAS rate, processed using Eq. (6) (lines). The optimized parameters are presented in Table 2.

where α is the angle of the instantaneous orientation of the dipole–dipole coupling tensor to the 'symmetry axis of fast motion' [32] or the polar angle between the internuclear vector $\boldsymbol{r}_{IS}$ and the end-to-end

Table 2. The nonlinear curve fitting parameter values of ^{1}H–^{13}C CP MAS kinetics in PDMAEMA (Fig. 3) and PMETAC (the experimental data from Ref. [8] were newly processed using Eq. (6)).

	PDMAEMA			PMETAC		
	N-$(CH_3)_2$	N-CH_2	O-CH_2	N^+-$(CH_3)_3$	N-CH_2	O-CH_2
A, s^{-1}	470	790	160	200	110	1200
B, s^{-1}	4500	17800	7100	4300	8200	10300
D_{CH}, Hz*	2900	16500	17600	1800	20800	21600
$R^{I}_{1\rho}$, s^{-1}	52	130	210	62	118	77
λ	0.43	0.33	0.33**	0.33**	0.33**	0.2
R^2/χ^2(%)	0.978/2.2	0.994/2.2	0.975/4.2	0.994/1.1	0.993/1.7	0.996/1.3

* The coupling constants D_{CH} were determined from b values, rescaling them by the factor of $\sqrt{2}$ because the HH matching for $n = +1$ was fulfilled (Eq. (4).

** The value $\lambda \approx 0.33$ was optimized for a I^{*}_{2}–S spin system and fixed in order to ensure the stable convergence of the nonlinear fitting flow.

vector of the polymer chain [35]. The static coupling constant D_{stat} for the ^{13}C–^{1}H dipolar coupling is usually taken as 23.0 ± 0.3 kHz that corresponds to the bond length r_{C-H} ~1.09–1.10 Å (Eq. (2)).

However, the above definitions of the angle α in Eq. (7) is unwelcoming for the visualization of the local disorder. The simplified visualization can be done if the internal motion of vector $\boldsymbol{r}_{IS}(t)$ is modelled as a restricted movement in a cone with the semi-angle θ_0. The order parameter is then given by $S = \cos\theta_0 (1 + \cos\theta_0)/2$ [31, 33]. The amplitude of this movement is qualitatively visualized by the cone semi-angle θ_0. The S and θ_0 values for the studied carbon sites in PDMAEMA are given in Fig. 4. These values significantly differ from those obtained for proteins, biological macromolecules and some more rigid systems [31, 33, 34].

Despite the wide use of quaternized PDMAEMA, and cationic polymers in general, there are few contributions related to investigations of quaternization reactions of tertiary amino groups and the properties of both forms. Therefore, the results

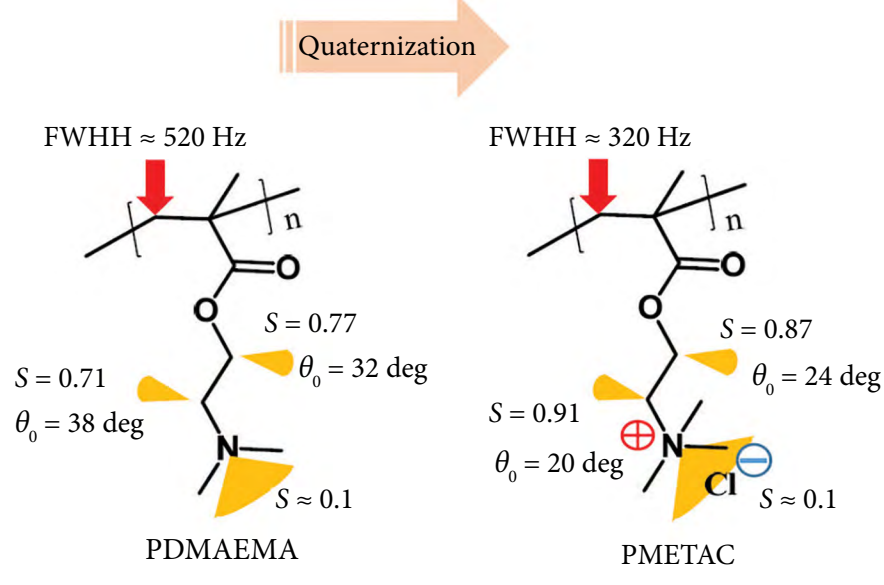

Fig. 4. The local dynamic disorder in PDMAEMA and PMETAC modelled as restricted movement of the internuclear vector $\boldsymbol{r}_{C-H}(t)$ in a cone: the order parameters S and the visualization of the local disorder for the studied carbon sites. The full widths at the half-height (FWHH) of the carbon signals in the main chain were determined separating the overlapped contours and approaching them by Voigt functions (Fig. 1).

obtained for PDMAEMA were compared with those for PMETAC, which is the quaternized derivative of PDMAEMA [8].

5.1. The ^{1}H and ^{13}C chemical shifts

The positional sequence of the signals in the ^{1}H NMR spectra is the same in both polymers (Fig. 2). This is in agreement with the solution (in $CDCl_3$) data [14, 15]. Also, the computed ^{1}H chemical shifts fairly well agree with the experiment. The assignments of ^{1}H peaks for PDMAEMA are taken from Ref. [14] and for one of its quaternized analogue (BuI-Q60) from Ref. 15]. The solid-state ^{13}C NMR spectra of the neat PDMAEMA and PMETAC were not found in the literature. Only the high resolution ^{13}C NMR spectrum of PDMAEMA in the DMSO-d_6 solution is presented in Ref. [11] and analyzed with the purpose to identify its stereochemical configurations. Therefore, it is interesting to note that the mutual interchange in the positions of N-CH_2 and O-CH_2 signals in the ^{13}C MAS NMR spectra of PDMAEMA and PMETAC is observed (Fig. 2). This means that the charge of the N^+ ion causes a very strong deshielding effect of the neighbouring carbon. The calculated ^{13}C chemical shifts also confirm this fact. However, the quantitative coincidence with the experimental spectra is not so perfect as in the case of protons.

5.2. The local disorder

The analysis of the dipolar coupling constants has revealed that the local disorder around various spin sites in PDMAEMA is significantly higher than in PMETAC (Fig. 4). Note that the local order around the N^+-CH_2 site in PMETAC is characterized by S = 0.91 that is intrinsic for quite rigid molecular systems [8, 33–35]. Hereby it is intriguing to compare the dynamic behaviour and disorder of the main chains. Unfortunately, there are strong overlaps of the CH_2 main chain signal with the neighbouring N-CH_2 peak in PDMAEMA (57 and 59 ppm, respectively (Fig. 1)) and that with the quaternary carbon (q) peak in PMETAC (46.5 and 45 ppm, see [8]). The signals can be separated applying the standard computing routines. Nevertheless, doing this, it has to be realized that the multi-parametrical curve fitting reduces the fidelity of deduced parameters. The overlapped experimental contours were separated using Voigt functions. The Voigt function is the convolution of Gauss (G) and Lorentz (L) profiles, i.e. $V = G * L$. It can be assumed that the presence of disorder enhances the Gauss contribution to the Voigt-shaped signals, whereas the Lorentz contribution is originated from the uniform spin interactions and dynamics. Gauss and Lorentz contributions (wG and wL) to the full width at the half-height (FWHH) of the main chain signal were found (Fig. 4). These are wG = 450 Hz and wL = 120 Hz for PDMAEMA and $wG \approx 0$ and wL = 320 Hz for PMETAC. This means that the main chain in PDMAEMA is highly disordered and more flexible than in PMETAC.

The local dynamic disorder of methyl groups attached to the nitrogen (N^+-$(CH_3)_3$ and N-$(CH_3)_2$) is extremely high in both polymers ($S \approx 0.1$). However, this result has to be treated with a certain reservation. The secularity condition $|b| \gg R^{I}_{df}$, R^{I}_{dp} is not fulfilled for these spin systems, and thus the use of the above models (Eq. (5) or (6)) is not rigorously legitimated. The ordering of CH_3 groups attached to the main chain was not studied as their signal consists of three peaks from stereochemicaly different forms (Fig. 1).

5.3. The spin dynamics

The rates of spin-lattice relaxation in the rotating frame and the anisotropy of spin-diffusion in PDMAEMA and PMETAC are found to be similar ($B/A \sim R^{I}_{dp}/R^{\Sigma}_{df} \sim 10 - 100$, $R^{I}_{1\rho} \sim 100$ s^{-1}, Table 2). The highest anisotropy in both polymers was found for CH_2 spins adjacent to the nitrogen.

6. Concluding remarks

The solid-state ^{1}H and ^{13}C spectra of the neat PDMAEMA were registered for the first time. The stereochemical content of PDMAEMA was determined from the complex shaped ^{13}C NMR signal of CH_3 group. The ^{1}H–^{13}C CP MAS HETCOR spectra have revealed the mutual interchange in the positions of N-CH_2 and O-CH_2 peaks in PDMAEMA and one of its quaternized analogue – PMETAC, whereas the sequences of proton signals are identical in both polymers. This experimental finding was confirmed by the DFT calculation.

The general Hirschinger and Raya spin dynamics solution was simplified and adapted for the spin cluster treatment. It was applied for the processing of the experimentally measured $^{1}H–^{13}C$ CP MAS kinetics in PDMAEMA and PMETAC. *A priori* constrains concerning the regime of the relaxation in the rotating frame are necessary for the precise determination of spin-diffusion rates. It was found that the rates of spin-lattice relaxation of protons and the anisotropy of spin-diffusion were very similar in both polymers.

The analysis of the dipolar coupling constants for various spin sites shows that the local disorder in PDMAEMA is significantly higher than in PMETAC. Moreover, the disorder in PDMAEMA increases going from the main chain along the pendant fragments. An opposite trend in PMETAC can be due to strong electrostatic interactions in the network of N^{+} and Cl^{-} ions that restrict the mobility of the pendant branches. It was also determined that the main chain in PDMAEMA is highly disordered and more flexible than in PMETAC.

Acknowledgements

The work is dedicated to Professor Jūras Banys on the occasion of his 60th anniversary. The authors acknowledge the Center of Spectroscopic Characterization of Materials and Electronic/Molecular Processes ('Spectroversum', http://spectroversum.ff.vu.lt) for the use of spectroscopic equipment. Computations were performed on resources at the High Performance Computing Center of Vilnius University ('HPC Sauletekis', http://supercomputing.ff.vu.lt). We thank Professor Jérôme Hirschinger for introducing us to the latest results obtained in his group at Strasbourg University prior to publication and for helpful discussions.

References

[1] J. Raya, A. Bianco, and J. Hirschinger, Kinetics of $^{1}H–^{13}C$ multiple-contact cross-polarization as a powerful tool to determine the structure and dynamics of complex materials: application to graphene oxide, Phys. Chem. Chem. Phys. **22**, 12209–12227 (2020).

[2] E.O. Stejskal and J.D. Memory, *High Resolution NMR in the Solid State: Fundamentals of CP/MAS* (Oxford University Press, New York, 1994).

[3] E.O. Stejskal, J. Schaefer, and J.S. Waugh, Magic-angle spinning and polarization transfer in proton-enhanced NMR, J. Magn. Reson. **28**, 105–112 (1977).

[4] V. Klimavicius, L. Dagys, and V. Balevicius, Subnanoscale order and spin diffusion in complex solids through the processing of cross-polarization kinetics, J. Phys. Chem. C **120**, 3542–3549 (2016).

[5] L. Dagys, V. Klimavicius, and V. Balevicius, Processing of CP MAS kinetics: towards NMR crystallography for complex solids, J. Chem. Phys. **145**, 114202 (2016).

[6] V. Klimavicius, A. Maršalka, A. Kizalaite, A. Zarkov, A. Kareiva, K. Aidas, J. Hirschinger, and V. Balevicius, Step-by-step from amorphous phosphate to nano-structured calcium hydroxyapatite: monitoring by solid-state ^{1}H and ^{31}P NMR and spin dynamics, Phys. Chem. Chem. Phys. **24**, 18952–18965 (2022).

[7] L. Dagys, S. Balčiūnas, J. Banys, F. Kuliešius, V. Chizhik, and V. Balevičius, CP MAS kinetics and impedance spectroscopy studies of local disorder in low-dimensional H-bonded proton-conducting materials, Lith. J. Phys. **59**, 130–138 (2019).

[8] V. Klimavicius, L. Dagys, V. Klimkevičius, D. Lengvinaitė, K. Aidas, S. Balčiūnas, J. Banys, V. Chizhik, and V. Balevicius, Solid-state NMR and impedance spectroscopy study of spin dynamics in proton-conducting polymers: an application of anisotropic relaxing model, J. Phys. Chem. B **125**, 12592–12602 (2021).

[9] L. Dagys, V. Klimkevičius, V. Klimavicius, S. Balčiūnas, J. Banys, and V. Balevicius, Cross-polarization with magic-angle spinning kinetics and impedance spectroscopy study of proton mobility, local disorder, and thermal equilibration in hydrogen bonded poly(methacrylic acid), J. Polymer Sci. **58**, 3253–3263 (2020).

[10] L. Dagys, V. Klimkevičius, V. Klimavicius, K. Aidas, R. Makuška, and V. Balevicius, CP MAS Kinetics in soft matter: Spin diffusion, local disorder

and thermal equilibration in poly(2-hydroxyethyl methacrylate), Solid State Nuclear Magn. Reson. **105**, 101641 (2020).

[11] J. Niskanen, C. Wu, M. Ostrowski, G.G. Fuller, S. Hietala, and H. Tenhu, Thermoresponsiveness of PDMAEMA. Electrostatic and stereochemical effects, Macromolecules **46**, 2331–2340 (2013).

[12] K.M. Huh, H.C. Kang, Y.J. Lee, and Y.H. Bae, pH-Sensitive polymers for drug delivery, Macromol. Res. **20**, 224–233 (2012).

[13] G. Kocak, C. Tuncer, and V. Bütün, pH-responsive polymers, Polym. Chem. **8**, 144–176 (2017).

[14] C. Bruce, I. Javakhishvili, L. Fogelström, A. Carlmark, S. Hvilsted, and E. Malmström, Well-defined ABA- and BAB-type block copolymers of PDMAEMA and PCL, RSC Adv. **4**, 25809–25818 (2014).

[15] M.A. De Jesús-Téllez, D.M. Sánchez-Cerrillo, P. Quintana-Owen, U.S. Schubert, D. Contreras-López, and C. Guerrero-Sánchez, Kinetic investigations of quaternization reactions of poly[2-(dimethylamino)ethyl methacrylate] with diverse alkyl halides, Macromol. Chem. Phys. **221**, 1900543 (2020).

[16] S. Agarwal, Y. Zhang, S. Maji, and A. Greiner, PDMAEMA based gene delivery materials, Mater. Today **15**, 388–393 (2012).

[17] V. Klimkevicius and R. Makuska, Successive RAFT polymerization of poly(ethylene oxide) methyl ether methacrylates with different length of PEO chains giving diblock brush copolymers, Eur. Polym. J. **86**, 94–105 (2017).

[18] M. Steponaviciute, V. Klimkevicius, and R. Makuska, Synthesis and properties of cationic gradient brush copolymers carrying PEO side chains and catechol moieties, Macromol. Chem. Phys. **222**, 2000364 (2021).

[19] V. Klimkevicius, M. Steponaviciute, and R. Makuska, Kinetics of RAFT polymerization and copolymerization of vinyl monomers by size exclusion chromatography, Eur. Polym. J. **122**, 109356 (2020).

[20] J.F. Hinton and K. Wolinski, in: *Theoretical Treatments of Hydrogen Bonding*, ed. D. Hadži (John Wiley & Sons, Chichester, 1997) pp. 75–93.

[21] M.J. Frisch, G.W. Trucks, H.B. Schlegel, G.E. Scuseria, M.A. Robb, J.R. Cheeseman, G. Scalmani, V. Barone, G.A. Petersson, H. Nakatsuji, et al., *Gaussian 16, Revision A.03* (Gaussian, Inc., Wallingford CT, 2016).

[22] K. Aidas, A. Maršalka, Z. Gdaniec, and V. Balevičius, A ^{13}C NMR and DFT study of critical behavior of binary water/2,6-lutidine solution, Lith. J. Phys. **47**, 443–449 (2007).

[23] L. Müller, A. Kumar, T. Baumann, and R.R. Ernst, Transient oscillations in NMR cross-polarization experiments in solids, Phys. Rev. Lett. **32**, 1402–1406 (1974).

[24] A. Naito and C.A. McDowell, Anisotropic behavior of the ^{13}C nuclear spin dynamics in a single crystal of L-alanine, J. Chem. Phys. **84**, 4181–4186 (1986).

[25] W. Kolodziejski and J. Klinowski, Kinetics of cross-polarization in solid-state NMR: a guide for chemists, Chem. Rev. **102**, 613–628 (2002).

[26] J. Hirschinger and J. Raya, J. Magn. Reson. Open (to be published).

[27] J. Raya and J. Hirschinger, Sensitivity enhancement by multiple-contact cross-polarization under magic-angle spinning, J. Magn. Reson. **281**, 253–271 (2017).

[28] J. Hirschinger and J. Raya, Analytical descriptions of cross-polarisation dynamics: relaxing the secular approximations, Mol. Phys. **113**, 3161–3175 (2015).

[29] C.A. Fyfe, A.R. Lewis, and J.M. Chézeau, A comparison of NMR distance determinations in the solid state by cross polarization, REDOR, and TEDOR techniques, Can. J. Chem. **77**, 1984–1993 (1999).

[30] V. Klimavičius, F. Kuliešius, E. Orentas, and V. Balevičius, Secular and semi-non-secular models of cross-polarization kinetics for remote spins: An application for nano-structured calcium hydroxyapatite, Lith. J. Phys. **61**, 27–34 (2021).

[31] A.G. Palmer III, J. Williams, and A. McDermott, Nuclear magnetic resonance studies of biopolymer dynamics, J. Phys. Chem. **100**, 13293–13310 (1996).

[32] K. Saalwächter and H.W. Spiess, in: *Polymer Science: A Comprehensive Reference*, Vol. 2 (Elsevier, 2012) pp. 185–219.

[33] J.L. Lorieau and A.E. McDermott, Conformational flexibility of a microcrystalline globular protein: order parameters by solid-state NMR spectroscopy, J. Am. Chem. Soc. **128**, 11505–11512 (2006).

[34] J.L. Lorieau and A.E. McDermott, Order parameters based on $^{13}C^{1}H$, $^{13}C^{1}H_2$ and $^{13}C^{1}H_3$ heteronuclear dipolar powder patterns: a comparison of MAS-based solid-state NMR sequences, Magn. Reson. Chem. **44**, 334–347 (2006).

[35] M. Wang, M. Bertmer, D.E. Demco, and B. Blümich, Segmental and local chain mobilities in elastomers by ^{13}C–^{1}H residual heteronuclear dipolar couplings, J. Phys. Chem. B **108**, 10911–10918 (2004).

SUKINIŲ DINAMIKOS IR LOKALIOSIOS NETVARKOS IŠMANIUOSIUOSE POLIMERUOSE TYRIMAS KIETOJO KŪNO BMR METODU: PDMAEMA

V. Klimavičius [a], V. Klimkevičius [b], L. Dagys [c], K. Aidas [a], R. Makuška [b], V. Balevičius [a]

[a] *Vilniaus universiteto Cheminės fizikos institutas, Vilnius, Lietuva*

[b] *Vilniaus universiteto Chemijos institutas, Vilnius, Lietuva*

[c] *NVision Imaging Technologies GmbH, Ulmas, Vokietija*

Santrauka

Ištirti kietojo kūno ^{1}H ir ^{13}C BMR spektrai bei ^{1}H–^{13}C CP („kryžminės poliarizacijos“) MAS („magiško kampo sukimo“) kinetika poli[2-(dimetilamino)-etilmetakrilate] (PDMAEMA), t. y. išmaniajame polimere, kuris pasižymi jautrumu pH ar temperatūros pokyčiams. Stereocheminė PDMAEMA sudėtis buvo nustatyta iš CH_3 grupių ^{13}C MAS signalo kontūro formos, atliekant persiklojusių smailių atskyrimą ir aproksimuojant jas Voigt funkcijomis. Eksperimentiniai CP MAS kinetikos duomenys buvo apdoroti taikant Hirschinger ir Raya sukinių dinamikos modelį, kuriame įtraukta pilnoji sukinių ir gardelės relaksacijų schema. Bendroji kinetinė lygtis buvo adaptuota sukinių spiečių nagrinėjimui. Siekiant palyginti, buvo peržiūrėti eksperimentiniai anksčiau tirtos CP MAS kinetikos poli[2-(metakriloiloksi)etiltrimetilamonio chloride] (PMETAC), t. y. vienoje iš kvaternizuotų PDMAEMA formų, duomenys ir apdoroti pritaikius šį modelį. Nustatytos ir palygintos sukinių difuzijos bei sukinių ir gardelės relaksacijų spartos, taip pat ^{1}H ir ^{13}C sukinių sąveikos konstantos. Pastarieji duomenys buvo naudojami dinaminiams lokaliosios tvarkos parametrams įvertinti. Aptikta anomaliai didelė sukinių difuzijos anizotropija; ji didžiausia CH_2 grupėms, esančioms šalia azoto atomų. Tai būdinga sukinių sistemoms, kuriose dominuoja Ising tipo sąveika. Nustatyta, kad protonų sukinių ir gardelės relaksacijos spartos abiejuose polimeruose yra panašios, ir šie vyksmai yra milisekundžių eilės. Lokalioji netvarka PDMAEMA yra žymiai didesnė. Ji apibūdinama lokaliosios tvarkos parametrais 0,71–0,77 PDMAEMA fragmentams ir atitinkamai 0,87–0,91 PMETAC fragmentams. Nustatyta, kad pagrindinė PDMAEMA grandinė taip pat labiau netvarki ir lankstesnė nei PMETAC.